# Strongly Correlated Confined Electrons

W. Häusler

I. Institut für Theoretische Physik,
Jungiusstr. 9, 20355 Hamburg, F. R. G.

**Summary:** A few-electron system, as realized in semiconducting quantum dots, is investigated. Numerical results for the charge density distribution in quasi one-dimensional (1D) systems reveal three characteristic regimes of electron densities. At low carrier densities the ground state and the collective excitations correspond to those of a finite Wigner crystal. At intermediate densities low energy excitations involving the spin occur in 1D and 2D. They are investigated using correlated "pocket state" basis functions. For non-isotropic confining potentials and sufficiently large mean electron distances $r_s$ this method becomes exact. The ratios between the lowest energy excitation energies are determined quantitatively using group theoretical methods. They are independent of the detailed form of the electron-electron repulsion potential and of $r_s$. The results of the pocket state apprach are compared with available numerical data. Transport through a quantum dot is investigated under Coulomb blockade conditions for weak coupling to perfect leads. A master equation approach allows to incorporate nonequilibrium properties at finite applied voltages as well as spin selection rules for the transitions between the correlated many electron states. A model for the recently discovered negative differential conductances is proposed. Asymmetries in the transport is predicted for asymmetric dot-lead coupling. Recent experimental results for in-plane magnetic fields can be described by the Zeeman-splitting of the many electron states.

## 1 Introduction

At very low charge densities the interaction energy of an electron system can be lowered by localizing the electrons at maximal distances. This leads to inhomogeneous charge density distributions (Wigner crystallization) at sufficiently large mean electron distances $r_s$ and has been predicted already in [1]. In the low density limit the electrons can be treated as classical particles repelling each other by Coulomb forces. Fermi statistics and electron spin are unimportant. Linearizing the inter electron forces for small deflections leads to phonon-like low energy excitations of the Wigner crystal. They correspond to vibrations of the electrons around their equilibrium positions and obey Bose statistics.

The argument of the more rapidly decreasing kinetic energy compared to the interaction ensures only the asymptotic existence of the Wigner crystal. Lower bounds for the required $r_s$-values are not easy to obtain. Up to now the most reliable values in three spatial dimensions (3D) are from Monte Carlo calculations [2] and yield $r_s \gtrsim 100\, a_B$. The Bohr radius $a_B = \varepsilon\hbar^2/me^2$ (which depends on material through the dielectric constant $\varepsilon$ and the effective mass $m$) establishes a natural length unit in presence of Coulomb interactions. In 1D a similar "critical" $r_s$-value of $100\, a_B$ has been estimated recently from numerical diagonalization data [3]. In literature the existence of a Wigner

crystal is frequently assumed [4, 5] e.g. in oder to calculate conductance properties of 1D systems. If these systems are finite [5], they can be models for *quantum dots*.

Semiconducting islands that are only weakly coupled to electron reservoirs by high tunneling barriers show single electron effects in transport related to small capacitances and Coulomb interactions. Coulomb blockade [6, 8] and periodic conductance oscillations are well known examples [7, 8, 9, 10, 11, 12]. The number of conducting electrons $N$ that are confined within GaAs/AlGaAs heterostructure quantum dots may be very low. Systems containing $N \leq 3$ electrons were even realized [13]. They can be considered as "artificial atoms" [14].

In the low density limit the energies do not depend on the spin. They are therefore $2^N$-fold degenerate. The first quantum mechanical correction with increasing density is a splitting of the vibrational levels into multiplets. In the absence of spin-orbit coupling, like in GaAs/AlGaAs, the total spin $S$ is still a good quantum number even in the presence of $e^- - e^-$ interaction. Therefore each sub-level has a well defined total spin $S \in \left\{ \left\{ \begin{matrix} 0 \\ 1/2 \end{matrix} \right\}, \ldots, N/2 \right\}$ for $N$ $\left\{ \begin{matrix} \text{even} \\ \text{odd} \end{matrix} \right\}$.

A main purpose of the present article is to describe this fine structure at intermediate electron densities. This cannot been done in terms of one-electron states where expectation values of the $(N-1)$ remaining electrons determine an effective (mean) field (cf. Section 3.2). A new method will be introduced to treat the many body problem in the presence of strong interactions. A set of highly correlated basis states will be used. Group theory will be applied to the problem and allows to select the physically relevant Fermionic states.

Transitions between the energy levels within the multiplets are the excitations with lowest energies. The following interesting properties will be demonstrated :

1. The fine structure excitation energies scale exponentially with $r_s$ and not according to a power law.

2. For given electron number and shape of the quantum dot the spectrum depends only on *one* parameter. The ratios between different excitation energies within one multiplet universally depend neither on $r_s$ nor on the detailed form of the $e^- - e^-$ repulsion.

3. Transitions between fine structure levels can be accompanied with changes in the spin of the electron system. Therefore, nonlinear transport, which is determined by the excitations of the quantum dot electrons [10, 11, 15, 16] is strongly influenced by the spin [17, 18].

4. When a particular dot symmetry is absent the state $S = N/2$ with all spins in parallel has the highest energy within the lowest vibrational multiplet and in 1D the ground state is always of minimal spin $S = \left\{ \begin{matrix} 0 \\ 1/2 \end{matrix} \right\}$ for $N$ $\left\{ \begin{matrix} \text{even} \\ \text{odd} \end{matrix} \right\}$.

5. In 2D the spins of the ground states corresponding to successive electron numbers $N-1$ and $N$ can differ by more than $1/2$. This influences even the linear conductance and crucially the nonlinear transport properties [19].

Increasing charge density reduces the strength of the Coulomb interaction compared to the kinetic energy. The electrons become delocalized. Then effective single particle treatments, like Hartree-Fock, become reliable and serve as justification of the charging model [15, 20] that describes successfully single electron effects in small metallic

islands. Comparisons between selfconsistent Hartree-Fock and numerical calculations show the importance of correlations.

## 2 Model

The $N$-electron quantum dot without magnetic field is described by the Hamiltonian

$$\begin{aligned} H &= \sum_{i=1}^{N} \left( \frac{\boldsymbol{p}_i^2}{2m} + v(\boldsymbol{x}_i) \right) + W(\boldsymbol{x}_1 \ldots \boldsymbol{x}_N) \\ W(\boldsymbol{x}_1 \ldots \boldsymbol{x}_N) &= \frac{1}{2} \sum_{\substack{i,j \\ i \neq j}} w(|\boldsymbol{x}_i - \boldsymbol{x}_j|) \quad . \end{aligned} \tag{1}$$

$\boldsymbol{x}_i$ and $\boldsymbol{p}_i$ in $d$ dimensions describe position and momentum of the $i$-th electron with (effective) mass $m$ carrying a spin $s$. Both the confinement potential $v(\boldsymbol{x})$ and the interaction $w(\boldsymbol{x})$ do not depend on spin. The 2D-case $v(\boldsymbol{x}) \sim \boldsymbol{x}^2$, $w(|\boldsymbol{x}|) \sim 1/|\boldsymbol{x}|$ has been investigated in detail for $N = 2$ [21, 14] and $N = 3$ [22] electrons. In Section 6.2 we will discuss a square shaped quantum dot with hard wall potential [23].

The case of a 1D square well of length $L$

$$\begin{aligned} v(x) &= V_0 \Theta(|x| - L/2) \quad , \qquad V_0 \gg \pi^2 N^2 / m L^2 \\ w(x) &= e^2 \frac{\mathrm{e}^{-\alpha|x|}}{\varepsilon \sqrt{x^2 + \lambda^2}} \quad , \qquad \lambda \ll L \end{aligned} \tag{2}$$

has been studied in [3, 24, 25] for $N \leq 4$, model (2) will be the example considered in Section 4. A (small) transversal spread of the wave functions is taken into account by $\lambda$ and $\alpha^{-1}$ is the range of the interaction.

## 3 Numerical Methods

### 3.1 Diagonalization

Model (2) has been investigated by numerical diagonalization in the basis of Slater determinants constructed from the eigenstates of the square well [3, 24, 25]. The number of one-particle states taken into account was $M \leq 13$. At large mean inter-electron distance $r_s \equiv L/(N-1) \gtrsim 100\, a_B$ the ground state probability density distribution is inhomogeneous and shows $N$ well separated peaks for $\alpha = 0$ (*Wigner molecule*), Figure 1. A similar behaviour has been found for the pair correlation function for a 2D quantum dot with harmonic potential in 2D [26].

This behaviour, which is characteristic for the regime where the Coulomb energy dominantes the kinetic energy, corresponds to Wigner crystallization. The charge density between the peaks is close to zero [3]. The full quantum mechanical ground state energy at large $r_s$ is therefore better approximated by equidistantly located classical point charges than by a homogeneous charge distribution [25].

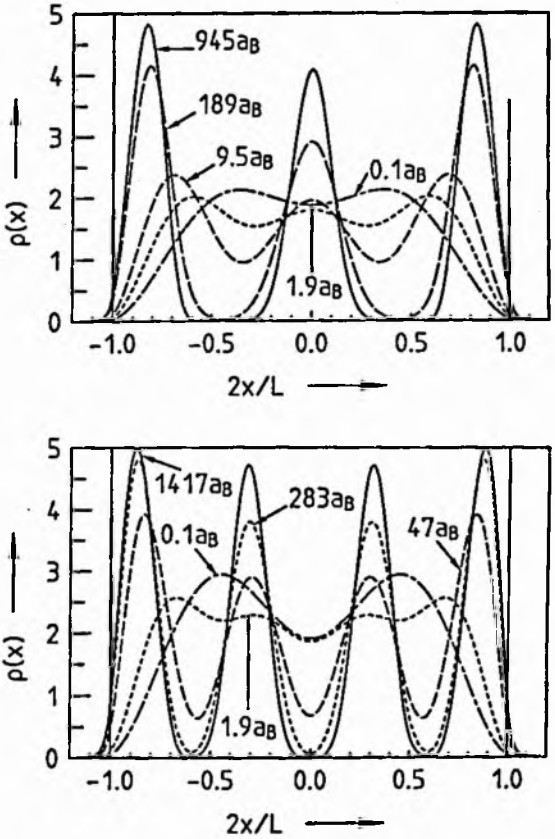


**Figure 1**
(a) Charge density $\varrho(x)$ of model (2) for $N = 3$ and (b) $N = 4$ for different $L$, normalized to $\int dx\, \varrho(x) = N$. When $L \gtrsim (N-1)a_B$ $N$ peaks begin to emerge. For $L \gtrsim 100(N-1)a_B$ the peaks are well separated. The non-vanishing density outside $\pm 1$ is due to a finite $V_0$ taken in (2).

The pronounced separation of the electrons is only found if $r_s < \alpha^{-1}$ (cf. (2)). For finite range $\alpha^{-1} < \infty$ of the interaction the charge density distribution at $r_s > 1\, a_B$ still shows $N$ peaks but does not approach zero even if $r_s > 100\, a_B$. As in 3D [27], the excitations in the low density limit correspond to vibrations of the charges around their equilibrium positions due to the Coulomb forces between them. The excitation energies $\Omega$ scale as $r_s^{-\gamma}$ with $\gamma \approx 3/2$ [25], Figure 2. For $r_s \gtrsim 100 a_B$ the spectrum is independent of whether the particles are Fermions or Bosons, cf. Section 5. At intermediate mean electron distances $1\, a_B < r_s < 100\, a_B$ the charge density distribution still differs from the non-interacting case ($r_s = 0.05\, a_B$ in Figure 1) and shows $N$ peaks. This is the regime where splittings of the vibrational levels are found. Typical spectra of model (2), obtained by numerical diagonalization, are shown in Figure 3. The multiplet structure is magnified. Each vibrational level, including Zeeman degeneracy has a total of $2^N$ states. The exponential $r_s$-dependence on the fine structure excitation energies is shown in Figure 4. It will be traced back to an overlap integral in Section 4. The ratios between these excitation energies can be calculated analytically for $N \leq 4$.

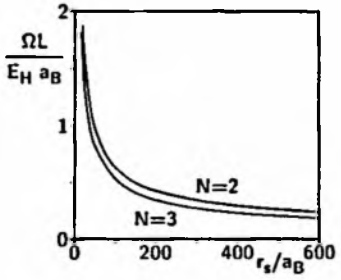


**Figure 2**
Energy difference $\Omega$ between the two lowest multiplets in units of $E_{\mathrm{H}}(a_{\mathrm{B}}/L)$ versus the mean electron distance $r_s$ for $N = 2$ and $N = 3$. The "Hartree" $E_{\mathrm{H}} \equiv e^2/a_{\mathrm{B}}$ is a natural energy unit. For $r_s \gtrsim 100\, a_{\mathrm{B}}$ the asymptotic behaviour is recovered.

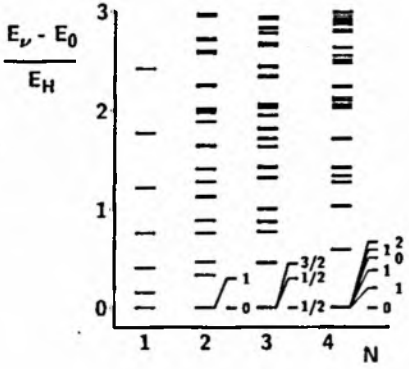


**Figure 3**
Typical spectra of model (2) for $N = 1, \ldots, 4$ and $L = 9.45 a_{\mathrm{B}}$. For $N \geq 2$ the low lying eigenvalues form groups of (fine structure) multiplets, the total number of states per multiplet being equal to the dimensionality of the spin Hilbert space $2^N$. For clarity the lowest multiplets are magnified indicating the total spin of each level. The ground state energies are subtracted.

## 3.2 Hartree-Fock Approximations

For most purposes the $N$-electron system in real atoms is satisfactorily described in terms of orbitals. Excitation energies correspond to transitions of single electrons between these one-electron states. The question arises, in how far this (effective) single particle picture is appropriate also for artificial quantum dot atoms with their reduced spatial dimensionality and density.

The Hartree-Fock procedure, if performed selfconsistently, leads to optimal single particle wave functions $\varphi_m$ for the interacting problem in the sense of a variational principle. The index $m$ includes both spatial and spin quantum numbers. An electron occupying the state $\varphi_m$ is influenced by all $N-1$ other electrons via the effective (Hartree-) molecular field, being proportional to their charge density [28]. These fields depend on the considered state $\varphi_m$ and in finite systems the term $m = m'$ has to be omitted from the molecular field

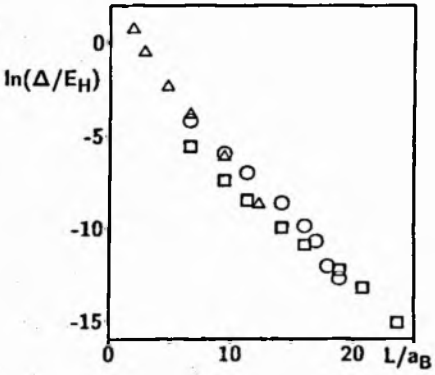


**Figure 4** Logarithm of the energy difference $\Delta$ between the ground state and the first excited state within the lowest multiplet versus the system length for $N = 2$ (□), $N = 3$ (○), and $N = 4$ (△).

$$v_{\mathrm{H}}^{(m)}(x) = \sum_{\substack{m'=1 \\ m' \neq m}}^{N} \int \mathrm{d}x' \, |\varphi_{m'}(x')|^2 \, w(|x - x'|) \quad . \tag{3}$$

Furthermore, the antisymmetrization requirement is taken into account via Slater determinants

$$\frac{1}{\sqrt{N!}} \begin{vmatrix} \varphi_1(x_1) & \dots & \varphi_N(x_1) \\ \vdots & \ddots & \vdots \\ \varphi_1(x_N) & \dots & \varphi_N(x_N) \end{vmatrix} \quad .$$

This leads to the additional non-local exchange potential

$$v_{\mathrm{E}}^{(m)}(x) = - \sum_{\substack{m'=1 \\ m' \neq m}}^{N} \int \mathrm{d}x' \, \varphi_{m'}^*(x) \varphi_{m'}(x') \, w(|x - x'|) \, . \tag{4}$$

The $\varphi_m(x)$ have to obey the effective one-electron Schrödinger equation

$$\left[ \frac{p^2}{2m} + v(x) + v_{\mathrm{H}}^{(m)}(x) + v_{\mathrm{E}}^{(m)}(x) \right] \varphi_m(x) = \epsilon_m \varphi_m(x) \tag{5}$$

where the fields $v_{\mathrm{H}}^{(m)}(x)$ and $v_{\mathrm{E}}^{(m)}(x)$ have to be determined selfconsistently. Iterating (3), (4) and (5) gives the ground state energy

$$E = \sum_{m}^{N} \left[ \epsilon_m - \frac{1}{2} \sum_{\substack{m'=1 \\ m' \neq m}}^{N} \int \mathrm{d}x \, \mathrm{d}x' \, w(|x - x'|) \right.$$
$$\left. \times \left( |\varphi_m(x)|^2 |\varphi_{m'}(x')|^2 - \varphi_{m'}^*(x) \varphi_m^*(x') \varphi_{m'}(x') \varphi_m(x) \right) \right] .$$

Hartree-Fock and numerically exact results were compared in detail for $N = 2$ electrons in a 2D quantum dot with parabolic confinement potential [28]. The authors have analyzed the ground state energy and the one- and two-particle densities at intermediate mean electron separations. Within Hartree-Fock approximation these quantities differ considerably from their exact values, in particular for the spin singlet state $S = 0$. The Hartree-Fock ground state can be even of wrong symmetry $S = 1$.

A similar behaviour is found for a 1D tight binding model with nearest and next nearest neighbour interaction [29]. Again a spin polarized ground state is favoured. This result contradicts to the rigorous theorem [30] where for interacting spin $s = 1/2$ Fermions in 1D an unpolarized ground state has been proven.

These results motivate a description of quantum dot electrons without using one-electron states but starting from a basis that includes correlations.

## 4 Pocket State Approximation

In this section the correlated $N$-electron basis functions will be introduced. They allow to calculate the fine structure spectra. The inhomogeneous density distribution (Figure 1) already suggests that localized amplitudes should be appropriate.

Let us at first assume $N$ distinguishable particles and ignore their spin. In Section 5 statistics and spin will be introduced. The motion of $N$-particles can be described as the motion of one particle in a configuration space of $N \cdot d$ dimensions. The confining potential $v$ in (cf. (1)) restricts the motion to a finite volume where the interaction $W(\vec{x})$ ( $\vec{x} \equiv \{x_1, \ldots, x_N\}$ ) corresponds to a certain potential energy. The quantum mechanics of this particle is equivalent to the solution of (1) for $N$ (distinguishable) particles.

Let us now concentrate on the 1D square well model (2) in order to discuss the properties of the potential and to describe the method. The configuration space is a (hyper-) cube of volume $L^N$. The repulsive interaction $W(\vec{x})$ separates different potential minima by barriers (at least of height $e^2/\lambda$). In the absence of additional symmetries of the single electron potential $v$, as is the case in 1D, there are $N!$ minima which are equivalent for like particles. They can be transformed into one another by permutation of their coordinates. In 2D the number of minima can be a multiple of $N!$. This case will be considered in Section 6.2. The minima are located on a hyper ring (a $(N-2)$-dimensional manifold) perpendicular to the main diagonal of the $L^N$-hyper cube. The center of the ring coincides with the center of the cube. Each of the minima is surrounded by $N-1$ nearest neighbouring minima at equal distances.

The one particle quantum mechanics of this potential with equivalent minima can be approximated similar to the text book treatment of the symmetric double well with a potential $V(x) = V(-x)$, sketched in Figure 5. The Hilbert space is restricted to the two "pocket" states $|L>$ and $|R>$ each localized around one of the minima of $V$. Time reversal symmetry is not broken, therefore $0 \leq <x|L> = <-x|R>$. The ground state and the first excited state are approximated by a symmetric and an antisymmetric linear combination of the basis functions, respectively. The energy difference $\Delta$ between the corresponding eigenvalues is proportional to the tunneling matrix element $<L|H|R>$ of the Hamiltonian. This approximation is good for a high barrier between both potential minima so that

$$\Delta \ll \Omega \tag{6}$$

where $\Omega$ is the energy of higher excitations of the double well system. In order to describe the higher excited states nodes have to be introduced which cannot be approximated by $|L>$ and $|R>$. Due to the exponential decay of $<x|L>$ and $<x|R>$ under the

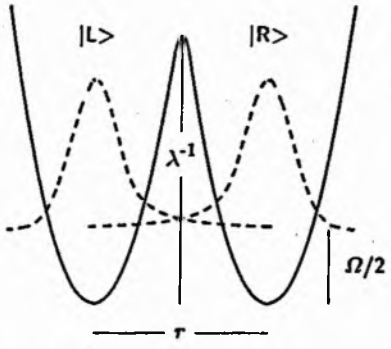


**Figure 5**
Double minimum potential, schematically. If $<L|H|R> \ll \Omega$ the Hilbert space can be restricted to span($|L>, |R>$) to describe the lowest excitation.

barrier, $\Delta$ is decreasing exponentially with increasing distance $r$ between the minima and $\Delta \sim \exp(-\lambda^{-1/2})$ with increasing height $\lambda^{-1}$ of the barrier. If $\Omega$ decreases only algebraically with $r$ (6) is fulfilled always at sufficiently large $r$. This justifies the truncation of the Hilbert space to span($|L>, |R>$) generated by two basis vectors.

The case in $L^N$ can be treated analogously, the pocket state approximation is not restricted to one-dimensional or translationally invariant (tight binding) potentials [31]. The Hilbert space is truncated to span($\{|p>\}$) generated by $N!$ basis states, each being strongly peaked around a certain potential minimum in coordinate representation $<x_1, \ldots, x_N|p>$, and small elsewhere. The ground state has the same symmetry as the Hamiltonian and is given by the symmetric linear combination

$$\frac{1}{\sqrt{N!}} \sum_{p=1}^{N!} |p> \quad . \tag{7}$$

The inhomogeneous charge density

$$\rho(x) = \frac{1}{(N-1)!} \times \sum_{p,p'} \int dx_2 \ldots dx_N <x, x_2 \ldots, x_N|p><p'|x, x_2 \ldots, x_N> \tag{8}$$

obtained in [3] reflects the separation of different probability amplitudes $<x_1, \ldots, x_N|p>$.

The one-to-one correspondence between the pocket states $|p>$ and permutations $p \in S_N$ is established via the multiplication

$$p'' = p \cdot p' \quad \Leftrightarrow \quad <x_1, \ldots, x_N|p''> = <x_{p(1)}, \ldots, x_{p(N)}|p'>$$

where $p(i)$ is a permutation of the sequence $i = 1, \ldots, N$. All pocket states are of equal shape due to the equivalence of the potential minima.

The $\{|p>\}$ constitute a regular representation of $S_N$ and thus the frequency for the occurrence of each irreducible representation (IR) $\Gamma$ is equal to the dimension $d_\Gamma$ of $\Gamma$. The construction of symmetrized functions by means of projectors

$$P_\Gamma := \sum_{p \in S_N} \chi^\Gamma(p) \mathcal{O}(p) \tag{9}$$

is facilitated through the (real) characters $\chi^\Gamma(p)$ of $S_N$ (cf. Section 5). The $\chi^\Gamma(p)$ are tabulated e.g. in [32] up to $S_7$. $\mathcal{O}(p)$ performs the permutation $p$ on the basis vectors $\{|p>\}$. The Hamiltonian matrix in the symmetrized basis

$$P_\Gamma \text{ span}(\{|p>\}) \tag{10}$$

is block diagonal.

The matrix elements $H_{pp'} \equiv <p|H|p'>$ describe the *correlated* tunneling between two different arrangements $p$ and $p'$ of the $N$ particles in (1). In contrast to effective single electron states the basis $\{|p>\}$ inherently takes correlations into account. The off-diagonal elements $H_{pp'}$ with $p \neq p'$ determine the differences between the eigenvalues of $H$ in the basis $\{|p>\}$ because the $H_{pp}$ are independent of $p$. Due to the exponential decay of $<x_1, \ldots, x_N|p>$ under the barriers, the $H_{pp'}$ scale roughly as $\exp(-r_s/r_c)$ where $r_c$ separates the weak from the strong interaction regime. On the other hand $\Omega \sim r_s^{-\gamma}$ and thus (6) is fulfilled at sufficiently low electron densities $r_s^{-1} < r_c^{-1}$. The exponential decay with $r_s$ furthermore allows to restrict the consideration only to $H_{pp'}$ with $p$ and $p'$ being nearest neighbours in $L^N$. For each $p$ there are $N-1$ nearest neighbours. These most important non-vanishing $H_{pp'}$ can shown to be equal to a good approximation.

The positions $\vec{x}^{(p)} \equiv (x_1^{(p)} \ldots, x_N^{(p)})$ and $\vec{x}^{(p')}$ of adjacent potential minima in $L^N$ differ only in one transposition of two coordinates $x_i^{(p)}$ and $x_j^{(p)}$ with $|x_i^{(p)} - x_j^{(p)}| = \sqrt{2} r_s$. Thus the dominant $H_{pp'}$ corresponds to an exchange of adjacent electrons in the original $N$-electron chain (Figure 1). From a particular minimum $\vec{x}^{(1)} = (0, r_s, \ldots, (k-1)r_s, kr_s, \ldots, (N-1)r_s)$, $1 \leq k \leq N-1$, a nearest neighbouring $\vec{x}^{(2)}$ is reached by inter-changing $x_{k-1}^{(1)}$ and $x_k^{(1)}$ at the position $k$. Due to the long range character of the Coulomb interaction the value of the corresponding overlap integral may depend on the position within the chain $k$. The relative magnitude of the $k$-dependence of $H_{pp'}$ can be estimated within a (simplified) WKB approximation, taking into account only the exponential dependence on the barrier [33]

$$H_{pp'} \sim \exp - \int_0^T \mathrm{d}\tau \left( \frac{m}{2} (\dot{\vec{x}}(\tau))^2 + W(\vec{x}(\tau)) \right) . \tag{11}$$

The path $\vec{x}(\tau)$ connects $p$ at $\tau = 0$ with $p'$ at $\tau = T$ and minimizes the action in (11). $T$ is the period of that motion.

The task of finding the extremal path will be simplified by taking $\vec{x}(\tau)$ as a straight line that connects $p$ with $p'$. This assumption disregards the motion of other electrons during the time $T$, and can be justified for small values of $\lambda$ in (2) when the height of the saddle point of the potential is dominated by $\lambda^{-1}$ and motions of the other electrons lead to modifications of this value only by a small amount. In 2D situations (1) this "adiabatic" simplification is generally not valid.

The (imaginary) time integration (11) can be substituted by one coordinate integration parametrized as $0 \leq q \leq 1$

$$H_{pp'} \sim \exp\left[-\sqrt{2}\, r_s \int_0^1 \mathrm{d}q\, \sqrt{2m\,(W(\vec{x}(q)) - W(\vec{x}(0)))}\right] \tag{12}$$

by using that the energy $\frac{m}{2}\left(\dot{\vec{x}}(\tau)\right)^2 - W(\vec{x}(\tau)) = W(\vec{x}(0)) = W(\vec{x}(T))$ is conserved along $\vec{x}(\tau)$. The factor $\sqrt{2}$ accounts for the two masses that are carried from $p$ to $p'$. For the interaction $w(x) = \frac{e^2}{\varepsilon}(x^2 + \lambda^2)^{-1/2}$ in (2)

$$H_{pp'} \sim \exp\left[-A_{N;k}\sqrt{\frac{L}{a_B}\frac{2\varepsilon}{N-1}}\right] \tag{13}$$

where $A_{N;k}$ contains the $k$-dependence of the WKB-action associated with the interchange of adjacent electrons in the chain. The $A_{N;k}$ still weakly depend on $N$ and $\lambda$. The numerical data shown in Figure 4 at low densities agree with a $\log(\Delta) \sim -\sqrt{L}$ behaviour. In Figure 6 $A_{N;k}$ is plotted for various $N$ and $\lambda/L = 2 \cdot 10^{-4}$ as used in

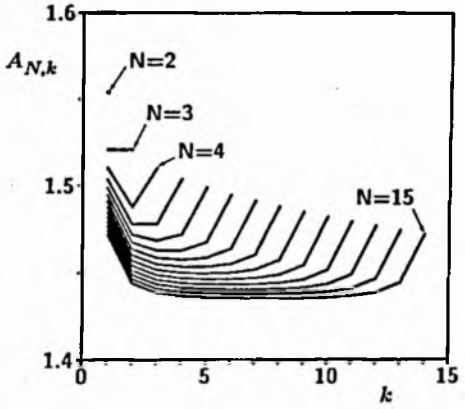


**Figure 6** $A_{N;k}$ as defined in the text versus the position $k$ along the chain for $\lambda/L = 2 \cdot 10^{-4}$ and various $N$.
The exchange of two adjacent particles close to the boundary leads to a slightly smaller overlap integral than other non-vanishing $H_{pp'}$. These variations with $k$ are negligible compared to the mean value of $A_{N;k}$.

Section 3.1. The variation of $A_{N;k}$ with $k$, less than 2% of its mean value, leads to significant $k$-dependences of $H_{pp'}$ only for $r_s \gtrsim 35 a_B$. But then $H_{pp'}$ has decreased to unobservable small values (cf. (wkblinear)) and the fine structure splitting disappears. The system consists of classical electrons (Wigner molecule). Increasing $\lambda/L$ to values up to 0.1 reduces the mean values of $A_{N;k}$ but leaves their relative variations with $k$ almost unaffected. If the interaction is modified by an additional cutoff (like in (2) when $\alpha > 0$) the $k$-dependence of $A_{N;k}$ becomes even smaller because the influence of other electrons on $W(\vec{x}(q))$ is smaller. This justifies to assume all non-vanishing

$H_{pp'} \equiv t_N$ to be equal for given electron number in 1D. The differences between the eigenvalues of $H$ within the lowest multiplets are then proportional to $t_N$ (Section 6.1) and their ratios independent of parameters like $r_s$, $\lambda$ or $\alpha$ (cf. (2)). Even the details of the whole shape of the inter-particle repulsion $w(x)$ does not influence these ratios. Insofar they are universal. In 1D only a non-zero range for the interaction is required to cause the exponentially small overlap between adjacent pocket states. The 2D case will be discussed in Section 6.2.

## 5 Symmetries

Up to now the quantum mechanics of $N$ distinguishable particles has been considered, ignoring their spin. This section is adressed to the question which of the $\Gamma$-symmetric eigenvectors of $H_{pp'}$ in the basis $\{|p>\}$ can satisfy the Pauli principle for physical systems of identical Fermions or Bosons with spins.

The indistinguishability of like particles requires that an eigenfunction

$$\psi(x_1\sigma_1, \ldots, x_N\sigma_N)$$

of (1) belongs to the one dimensional, (anti)symmetric irreducible representation (IR) of $S_N$ with respect to permutations among the *enumeration* of the particles. These permutations affect position $x_i$ and spin $\sigma_i$ of the $i$-th particle simultaneously.

Apart from this unalienable symmetry the Hamiltonian (1) (in absence of spin-orbit coupling) is furthermore invariant under *separate* permutations of the $\{\hat{x}_1 \ldots \hat{x}_N\}$ and $\{\hat{\sigma}_1 \ldots \hat{\sigma}_N\}$ operators. Therefore $\psi$ additionally transforms according to IR's $\Gamma_x$ and $\Gamma_\sigma$ of the group of permutations among the spatial and spin degrees respectively. Both permutation groups can be considered as isomorphous to $S_N$.

All irreducible representations $\Gamma$ of $S_N$ can be labeled by partitions

$$[n_1, \ldots, n_N] \tag{14}$$

of ordered sequences of positive integers obeying

$$n_i \geq 0\,, \quad \sum_{i=1}^{N} n_i = N\,, \quad n_i \geq n_{i+1} \quad \text{for} \quad 1 \leq i \leq N \quad .$$

E.g. $[1, \ldots, 1]$ and $[N]$ denote the antisymmetric and the symmetric IR respectively ($n_i = 0$ is usually not written). Notation (14) helps to characterize the symmetries of spin states, see below.

The only factor group of $S_N$ is isomorphous to $S_2$ implying the existence of an adjoined IR $\overline{\Gamma}$ to every $\Gamma$ of equal dimensionality and equal moduli for the characters $|\chi^{\Gamma}(p)| = |\chi^{\overline{\Gamma}}(p)|$. From the orthogonality relations among characters follows that Kronecker products

$$\Gamma_1 \times \Gamma_2 \quad \text{contain} \quad \left\{ \begin{matrix} [1, \ldots, 1] \\ [N] \end{matrix} \right\} \quad \text{only if} \quad \begin{cases} \Gamma_1 = \overline{\Gamma}_2 \\ \Gamma_1 = \Gamma_2 \end{cases} . \tag{15}$$

The Pauli principle requires that $\Gamma_x \times \Gamma_\sigma$ must contain the (anti)symmetric IR

$$\Gamma_x \times \Gamma_\sigma \times \left\{ \begin{matrix} [1,\ldots,1] \\ [N] \end{matrix} \right\} \neq \emptyset \quad \text{for} \quad \left\{ \begin{matrix} \text{Fermions} \\ \text{Bosons} \end{matrix} \right. . \tag{16}$$

Thus with (15) $\Gamma_\sigma = \overline{\Gamma}_x$ has to be fulfilled for Fermions and $\Gamma_\sigma = \Gamma_x$ for Bosons ($\psi$ is in general no product of a spatial and a spin function).

$\Gamma_\sigma$ cannot be any IR of $S_N$ with respect to permutations among $\{\sigma_1,\ldots,\sigma_N\}$. Only IR's of the type $\Gamma_\sigma = [n_1, n_2]$ (cf. (14)) can occur for $s = 1/2$ particles. The total spin $S$ is related to $n_1$ and $n_2$ through

$$\Gamma_\sigma = [n_1, n_2] = [N/2 + S\ ,\ N/2 - S] \tag{17}$$

and fixes therefore uniquely $\Gamma_x$. Special cases of (17) are $S = N/2$ (all spins coupled in parallel) $\Longrightarrow$ $\Gamma_\sigma = [N]$ and $\Gamma_x = [1,\ldots,1]$, or $S = 0$ (assume $N$ to be even) $\Longrightarrow$ $\Gamma_\sigma = [N/2, N/2]$ which is antisymmetric only for $N = 2$. Due to the latter property the lowest eigenvalue of $H_{pp'}$ (associated with a symmetric wave function) is allowed for not more than two Fermions.

The dimensions $d_{[n_1,n_2]}$ of the IR's (17) can be expressed explicitly [34]

$$d_{[N/2+S\ ,\ N/2-S]} = \frac{(2S+1)\,N!}{(N/2+S+1)!\,(N/2-S)!} \tag{18}$$

in terms of $N$ and $S$. It is equal to the frequency of appearances of IR $\Gamma = [N/2 + S\ ,\ N/2 - S]$ in a regular representation. Thus

$$d_{[N/2+S\ ,\ N/2-S]} \leq \kappa_{N,S} \tag{19}$$

gives a lower bound to the number $\kappa_{N,S}$ of different eigenvalues of the Hamilton matrix in the pocket state basis to a given total spin $S$. In absence of further symmetries in spatial space, like in 1D, (19) becomes an equality. Because of the $(2S+1)$-fold Zeeman degeneracy of each fine structure level

$$\sum_{S=0 \text{ or } 1/2}^{N/2} (2S+1)\, d_{[N/2+S\ ,\ N/2-S]} = 2^N$$

is equal to the dimensionality of spin space.

## 6 Results

It remains to diagonalize the individual blocks of the Hamiltonian matrix in the symmetrized basis (10). Up to $N \leq 4$ this can be performed analytically. For $N = 5$ and $N = 6$ the results are obtained by numerical diagonalization of the remaining blocks of size $5 \times 5$ and $9 \times 9$ respectively. This should be compared with the amount to diagonalize the full Hamiltonian, as discussed in Section 3.1. The matrices for $N = 4$ electrons are typically of size $15000 \times 15000$ to obtain accurate fine structures.

| $N$ | $S$ | $E_i^{(N)} - E_{\text{Bose}}^{(N)}$ |
|---|---|---|
| 2 | 0 | 0 |
| 2 | 1 | $2t_2$ |
| 3 | 1/2 | $t_3$ |
| 3 | 1/2 | $3t_3$ |
| 3 | 3/2 | $4t_3$ |
| 4 | 0 | $(3-\sqrt{3})t_4$ |
| 4 | 1 | $(4-\sqrt{2})t_4$ |
| 4 | 1 | $4t_4$ |
| 4 | 0 | $(3+\sqrt{3})t_4$ |
| 4 | 1 | $(4+\sqrt{2})t_4$ |
| 4 | 2 | $6t_4$ |

**Table 1** Analytical values for the fine structure spectrum $E_i^{(N)}$ of model (2) within PSA for $N \leq 4$. $S$ refers to the total spin of $N$ Fermions with $s = 1/2$. The excitation energies $E_i^{(N)} - E_{\text{Bose}}^{(N)}$ are given in units of $t_N$ and referred to the eigenvalue $E_{\text{Bose}}^{(N)}$ of the symmetric linear combination of pocket states (7) which corresponds to the $s = 0$ Bosonic ground state.

### 6.1 Quasi-1D

The analytically obtained fine structure spectra of model (2) are listed in Table 1. The lowest eigenvalue of $H_{pp'}$ is taken as ground state and the energies are measured in units of $t_N$. The spectra for $N = 5$ and $N = 6$ are included in Figure 7. To analyze the spectral properties of the Hamiltonian in the pocket state basis it is convenient to consider the matrix $M$ being defined through

$$M_{pp'} \equiv H_{pp'} - H_{pp}\delta_{pp'} \quad , \qquad H_{pp'} \equiv <p|H|p'> \quad . \tag{20}$$

A matrix proportional to the unit matrix has been subtracted from $H_{pp'}$ ($H_{pp}$ does not depend on $p$). $M$ is block diagonal simultaneously with $H$ in the basis (10). The trace of $M$ vanishes. If $p$ and $p'$ differ by an odd permutation (like a single transposition, cf. Section 4) – this is the case for all dominant $H_{pp'}$ discussed in this paper – each eigenvalue $\epsilon$ of $M$, associated with a $\Gamma$-symmetric eigenvector, has a counterpart $-\epsilon$ corresponding to an eigenvector of adjoined symmetry $\overline{\Gamma}$ (cf. Section 5). This follows from the property $\chi^{\overline{\Gamma}}(p) = \pm\chi^{\Gamma}(p)$ for the characters of $S_N$ depending of the parity of $p$. Thus the spectrum of $M$ is symmetrically distributed around $\epsilon = 0$. If the $M_{pp'}$ further have the property to be either zero or equal to one common constant $t_N$ (so that the rows and the columns of $M$ still represent $S_N$) all eigenvalues of $M$ are proportional to $t_N$. This is valid to good approximation, cf. Section 4. In Figure 7 eigenvalues of $H_{pp'}$ are shown which after (16) are compatible with the Pauli principle for Fermions. According to Section 5 the corresponding adjoined eigenvectors belong to $s = 1/2$ Bosons. Thus, together with (15), (16) and (17) the following interesting relationship is proven : If $\epsilon$ is the eigenvalue of $M$ to a Fermion state with a certain spin $S$ then $-\epsilon$ is eigenvalue to a Bose state with the same spin $S$ and vice versa.

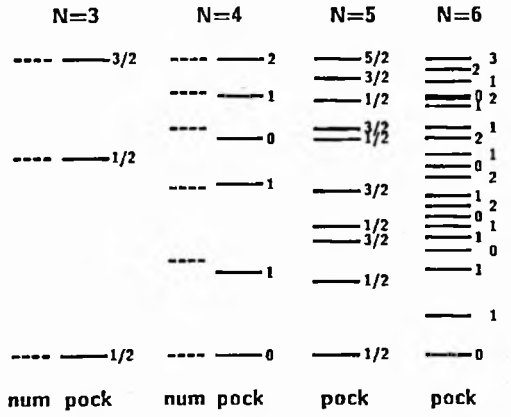


**Figure 7** Fine structure multiplets for $N = 3, \ldots, 6$ as obtained within PSA (**pock**). The numerical values (dashed) are obtained as in Section 3.1 (**num**) for systems of length $L = 11.3\, a_B$, $N = 3$ and $L = 13.2\, a_B$, $N = 4$. The $N$-dependence of $t_N$ is not considered, $t_N$ has been adjusted to normalize the overall width of the multiplets.

Knowing furthermore that the ground state of $H_{pp'}$ is symmetric (i.e. $\Gamma_x = [N]$, this is the $S = N/2$ Bose ground state) we have as corollary :

- The highest state within the lowest vibrational multiplet is the spatially antisymmetric Fermion state with $S = N/2$. This state occurs only once because $d_{[N]} = 1$ (cf. (18)).

It is only required that the pocket state basis forms a regular representation of $S_N$ and that the dominant $H_{pp'} = t_N$ connect permutations with different parity. The dimensionality of the quantum dot e.g. is not used. If the pocket state description is applicable and if $\nu = 1$ (cf. Section 6.2), the statement • is valid also in 2D situations.

In 1D has been shown [30] that

$$E(S) > E(S') \quad \text{if} \quad S > S' \tag{21}$$

where $E(S)$ is the lowest energy eigenvalue of the system to given spin $S$. The interaction $w(x)$ between the electrons is only required to be bounded and independent of spin. All fine structure spectra shown in Figure 7 obey (21). Though a Fermion ground state generally cannot be nodeless, cf. Section 5, its measure of zeros is minimal providing the totally antisymmetric transformation behaviour with respect to permutations of the particle enumeration. Its spin is either $S = 0$ or $S = 1/2$ depending on the parity of $N$. On the other hand the state with the largest measure of zeros is now found to be of highest energy within the lowest multiplet. This state of maximal spin plays a particular role for the nonlinear transport through a quantum dot [18], cf. Section 7. This state is obtained as ground state in calculations for spinless electrons. The spin degree of freedom allows the interacting electron system to lower its ground state energy. Recently this has been found also for the 3D Wigner crystal [35].

The numerical results (dashed lines in Figure 7) agree nicely with the pocket state approximation (PSA). Not only the sequence of spin values is described correctly but also quantitatively the ratios $\delta$ among the distances between the levels. The expo-

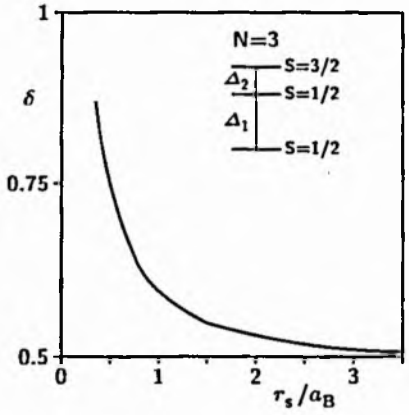


**Figure 8**
Numerically obtained ratio $\delta \equiv \Delta_2/\Delta_1$ of model (2) between the two fine structure energy differences $\Delta_1$ and $\Delta_2$ versus $r_s$ for $N = 3$ as indicated in the inset. According to the PSA $\delta = 1/2$, cf. Table 1. Below $r_s \lesssim 0.3\, a_B$ the third excited state is of spin $S = 1/2$ instead of $S = 3/2$ which makes the definition of $\delta$ ambiguous.

nential approach of the numerically obtained $\delta$'s to their "universal" values allows to deduce a scale $r_c$ for electron separations characterizing the transition from the almost non-interacting situation ( $r_s \ll r_c$ ) into the qualitatively different regime of strong correlations ($r_s \ll r_c$). In Figure 8 $\delta$ is taken as ratio between the two lowest excitation energies for $N = 3$. The obtained value $r_c \approx 2\, a_B$ agrees with the value extracted from the exponential decay of $\Delta_1$, cf. Figure 4, and extracted from the evolution of the charge density distribution into $N$ peaks, Figure 1.

The results presented in this section are valid in quasi-1D "slim" quantum dots if the width $b$ of the system does not exceed the width $u$ of the pocket state wave function. This follows from the requirement

$$\frac{\pi^2}{mb^2} \gg \Omega \sim \frac{1}{mu^2}$$

of large excitation energies in transversal direction compared to the vibrational energies.

At low densities the excitation spectra calculated in [23] for two electrons in a 2D rectangular square well box ($b = L/10$) look very similar to the 1D-spectrum for $N = 2$ in Figure 3. Only for very large electron separations $r_s = L > 3 \times 10^4\, a_B$, which have not been considered in [23], deviations would be expected due to the decreasing relative width $u$.

### 6.2 2D-Square

The pocket state description can be applied in 2D if two requirements are fulfilled :

1. the system has no continuous symmetry (the one-particle density shows peaks)
2. the $e^- - e^-$ interaction decays slower than $w(x) \sim x^{-2}$ with distance $x$.

Then all the qualitative results explained in the previous sections are valid also in 2D at low densities. The excitation spectrum shows phonon-like vibrational levels $\sim \Omega$ which split $\sim \Delta$ due to tunneling between different electron arrangements. The important difference to 1D is the reduced height of the potential barrier, the electrons can exchange their positions more easily by surrounding each other. Some of the paths connecting different arrangements involve merely slight changes in the electron distances, so that the tails of the long range Coulomb interaction creates only shallow barriers between the potential minima. Therefore a long range part of $w(x)$ is necessary in 2D, in contrats to 1D. Again the separation $\Delta \ll \Omega$ of energies is established at sufficiently large $r_s$ due to different scaling behaviours $\Delta \sim \exp(-r_s/r_c)$ and $\Omega \sim r_s^{-\gamma}$.

Numerical results for excitation spectra of electrons at low densities in rectangular quantum dots with hard wall potential are available only for $N = 2$ [23]. Figures 1 and 2 of [23] confirm the expected grouping of the levels with increasing system size $L$ into vibrational multiplets with internal structure. A considerably larger value for $r_c$ as compared to $2\,a_B$ can be estimated form these Figures.

The PSA has to be generalized to understand the case of a square shaped quantum dot, Figure 2 of [23]. The configuration space of the substitutional single particle (Section 4) now is a hyper cube of volume $L^{2N}$. In presence of $\nu$ degenerate classical ground state configurations for the repulsively interacting electrons the number of potential minima may be a multiple $\nu$ of $N!$. This is the case already for $N = 2$ where $\nu = 2$. The 4 pocket states describing two electrons in a square are represented in

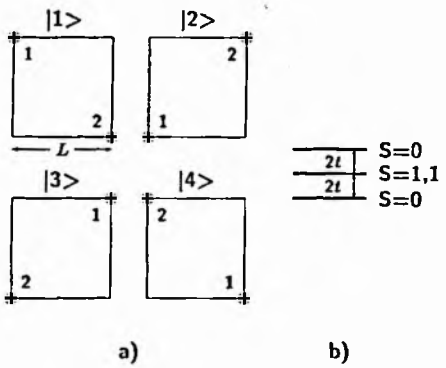


**Figure 9** a) The 4 equivalent arrangements of minimal inter-particle repulsion for $N = 2$ electrons on a square that determine the 4 pocket states in $L^4$.
b) The resulting fine structure spectrum consists of 3 levels at equal distances and total spins $S$ as indicated.

Figure 9 a. The dominant overlap integrals are of type $<1|H|2> = <1|H|3>$. Due to the larger tunneling path $<1|H|4>$, which corresponds to a permutation of two like particles, is much smaller. Neglecting overlap integrals of the latter type and classifying the obtained eigenstates according to their transformation properties with respect to *permutations among particle enumerations* leads to a fine structure spectrum as shown in Figure 9 b. The $\nu$-fold classical ground state increases the number of states in the multiplet to $\nu \cdot 2^N$, including Zeeman degenerated levels. For two electrons the ground

state is a symmetric linear combination of the 4 pocket states. The value $S = 0$ for the ground state spin can be explained easily (cf. [30]) even in arbitrary dimensions. The one-particle density (8) shows 4 peaks of equal weight in the 4 corners each containing a charge $e/2$. Removal of the square symmetry (cf. Section 8) would cause a splitting of the two degenerate $S = 1$ states.

Three electrons in the classical ground state configuration are again located in the corners of the square in $\nu = 4$ degenerated ways. Tunneling into the empty place is the dominant process. $4 \times 3! = 24$ pocket states determine the fine structure multiplet. The resulting spectra are shown in Figure 10 a). The multiplet contains in total $4 \times 2^3 = 32$ states. For four and five electrons in a square exists only $\nu = 1$ classical ground state

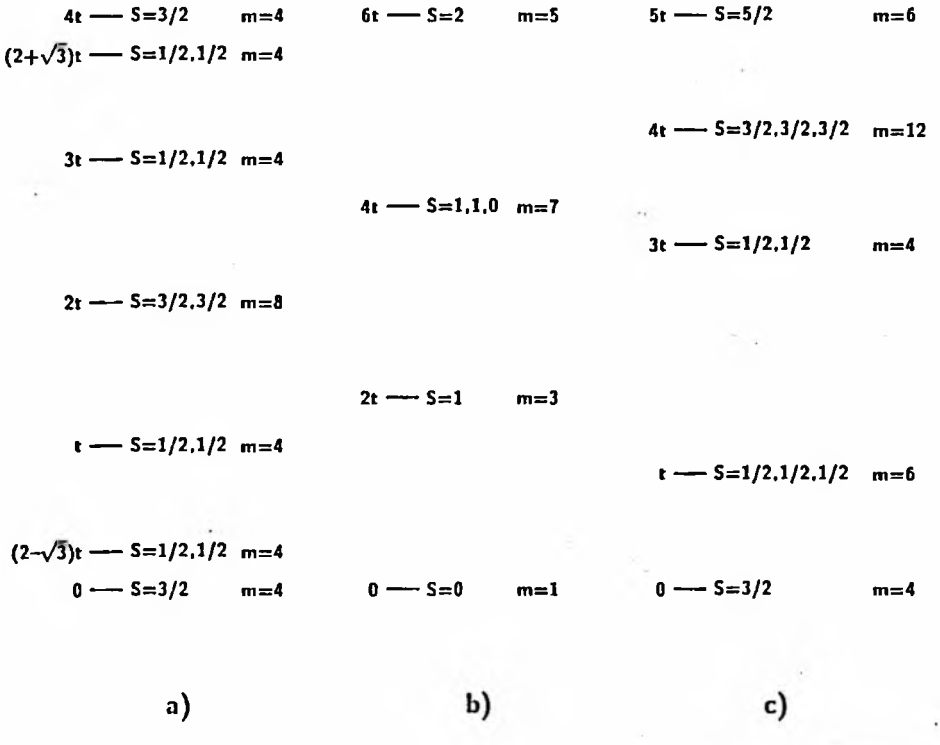


**Figure 10** Fine structure spectra of a) $N = 3$, b) $N = 4$, c) $N = 5$ electrons in a 2D square within PSA in units of $t$. The spin values $S$ and the number of states m per level are indicated. The dominating tunneling integrals $t$ are described in the text.

configuration. The number of pocket states is 4! and 5! respectively. For $N = 5$ the dominant tunneling process is the exchange of the central electron with one of the electrons located on the corners. This is the path of shortest length and involves only

two electron masses. The resulting fine structure is shown in Figure 10 c). For $N = 4$ two possible paths should be considered : $i$) rotation of all four electron positions simultaneously by 90° (ring exchange) $ii$) exchange of just two adjacent electrons leaving the remaining two unaffected. In one case the mass and in the other case the height of the potential barrier is larger. Assuming straight lines, like in (12), for the paths in $L^{2N}$ the action corresponding to $i$) can be expressed as a single integral yielding a numerical value $1.6\sqrt{\varepsilon L/a_B}$. In the second case the spatial trajectory, how the two electrons surround each other classically, is more difficult to determine. A rough estimate for the action is obtained by the following linear path for the pair exchange during the time $T$ : The first electron moves along one edge of the square, passing half the way at time $\tau = T/2$ while the second electron moves along two pieces of straight lines, bending halfway at the position of the lowest saddle point of the potential close to the center of the square. The action connected with this latter path yields a numerical value $1.1\,\hbar\sqrt{\varepsilon L/a_B}$. Both estimates are upper limits to the true classical imaginary time actions and the approximation $ii$) is surely worse compared to $i$). Therefore the exchange of adjacent electrons should be the slightly favourable process. Neglecting other processes leads to a fine structure spectrum for four electrons as it is shown in Figure 10 b). However, the difference between the two paths is not very pronounced so that entries due to the ring exchange into the Hamiltonian matrix can modify the $N = 4$ fine structure if $r_s = L$ is not very large.

As prominent property, in contrast to 1D, the ground state spin values in 2D are not minimal. The three electron ground state contains the polarized spin state $S = 3/2$ and the five electron ground state has even $S = 3/2$. This proves the non-applicability of the Lieb and Mattis-theorem [30] to higher dimensionalities if $N > 2$. Furthermore this property crucially influences nonlinear transport properties of quantum dots [19].

## 7 Nonlinear Transport

The transport behaviour of a quantum dot being only weakly coupled to left and right electron reservoirs by high tunneling barriers are determined by properties of the isolated dot. At small applied voltages and low temperatures the current is Coulomb blocked if left and right chemical potentials $\mu_L = \mu_R$ are not equal to the difference between $N$ and $N-1$ electron ground state energies $E_0^{(N)} - E_0^{(N-1)}$ (chemical potential of the dot). Otherwise the current is finite but the dot electron number can oscillate only between the two adjacent values $N$ and $N-1$ (SET oscillations, $N$ can be tuned through the external gate-voltage $V_G$ ).

At finite transport-voltages $V = (\mu_L - \mu_R)/e$ transitions between excited states $E_i^{(N)}$ and $E_j^{(N-1)}$ of the many electron system in the dot can additionaly contribute to the current. At zero temperature the current values jump step-wise with changing voltages. This allows the direct observation of dot spectra $E_i^{(N)}$. The current steps are, however, not necessarily positive with increasing transport-voltage !

The occurrence of negative differential conductances has been investigated in detail experimentally [16] and theoretically [18, 19]. They were traced back to spin selection rules. An entering or escaping electron can change the total spin of the correlated dot electron system only by $\pm 1/2$.

The nonlinear current is obtained from the non-equilibrium populations $P_i$. In contrast to [15] the index $i$ refers to the many electron dot levels (in Fock space) which

includes (i) electron number $N$, and at given $N$ (ii) the total spin $S$, (iii) its (Zeeman-) $z$-component and (iv) the energy level. The stationary dot populations are assumed to obey

$$\sum_{j,j\neq i} (\Gamma_{ij} P_j - \Gamma_{ji} P_i) = 0 \quad . \tag{22}$$

Here $\Gamma_{ij}$ denotes the rate for the transition from state $j$ to state $i$ which is associated either with entrance or escape of one single electron (two electron processes are suppressed for weak coupling between dot and leads). Passages through left or right barriers have to be added up. The transmittances $t_{\mathrm{L}}$ and $t_{\mathrm{R}}$ of the two barriers can be different (then the current is restricted mainly by the smaller $t_{\mathrm{L/R}}$); for simplicity the $t_{\mathrm{L/R}}$ are assumed to be independent of energy. The $\Gamma_{ij}$ further guarantee energy conservation. Entering or leaving electrons have to provide the transition energy $E_i - E_j$ between the involved dot states. The leads are assumed to be at thermal equilibrium without $e^- - e^-$ interactions. Then Fermi functions $f_{\mathrm{L/R}}$ and the density of lead states describe the energy distribution for entering electrons. Empty lead states for escape are available proportional to $(1 - f_{\mathrm{L/R}})$. $f_{\mathrm{L}}$ and $f_{\mathrm{R}}$ contain the temperature and the applied $\mu_{\mathrm{L}}$ and $\mu_{\mathrm{R}}$. A term proportional to $NeV_{\mathrm{G}}$ subtracted from the dot energies accounts for the applied gate-voltage.

One remark should be made about the validity of the rate equation description (22). Only in presence of phase randomizing processes, implicitly assumed in [36], the time evolution of the quantum dot is described by the diagonal elements of the dot density matrix (which are the level populations $P_i$) by the left hand side of equation (22). The phase randomizing processes provide the decay of the off-diagonal elements of the density matrix on time scales shorter than the times $(\sum_i \Gamma_{ij})^{-1}$ between successive electron passages through the barriers. If the barriers are too transmittive or in absence of any incoherencies, the time evolution of the full density matrix of the dot has to be taken into account.

Importantly, selection rules are taken into account for transitions that change the total dot spin from $S_i$ to $S_j$. The

$$\Gamma_{ij} \propto \begin{cases} \dfrac{S_j + 1}{2S_j + 1} & \text{for } S_i = S_j + \dfrac{1}{2} \\ \dfrac{S_j}{2S_j + 1} & \text{for } S_i = S_j - \dfrac{1}{2} \end{cases} \tag{23}$$

are assumed to be determined by the Clebsch-Gordan coefficients for coupling of angular momenta. In presence of a magntic field the spin states split into $(2S+1)$ Zeeman-levels and transitions are allowed only between adjacent $z$-components. These selection rules are essentially based on correlated many-electron states for the dot. Within the charging model the influence of the Coulomb interaction on the dot excitations is ignored and for individual electronic spins (23) becomes meaningless.

The spin selection rule (23) influences transport through two types of transitions (*i*) and (*ii*). (*i*) $\qquad N,\ S = N/2 \longrightarrow N-1,\ S'$

This electron escape transition, in contrast to all $S < N/2$ states, must reduce the dot spin $S' = (N-1)/2$. Furthermore, the Clebsch-Gordan coefficients favour allowed $S' > S$ transitions rather than $S' < S$. The $S = N/2$ state becomes stable over relatively long times (its occupation is supported by the Clebsch-Gordan coefficients) which causes a suppression of the current. This first type ($i$) of *spin blockade* [18] phenomenon starts to appear at transport-voltages of the order of the width of the lowest vibrational multiplet because the $S = N/2$ state is always one of the energetically excited states. For 1D and for $\nu = 1$ cases in 2D it has been shown (cf. Section 6.1) that this state is of highest energy in the lowest vibrational multiplet. This is the origin of negative differential conductances. The overall behaviour of the differential conductance versus

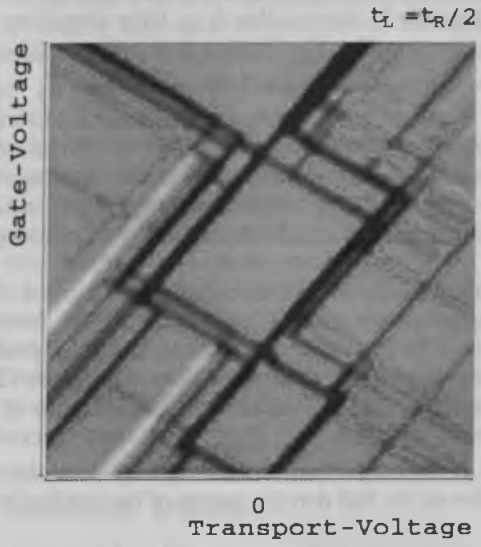


**Figure 11**
Differential conductance versus gate- $V_G$ and transport-voltage $V$. The zero-value inside the diamond shaped Coulomb blockade regions corresponds to grey. Dark and bright parts indicate positive and negative differential conductances, respectively. Bright regions are preferably found on one side of the transport voltage axis because the couplings between dot and the leads have assumed to be unequal $t_L = t_R/2$.

gate-voltage $V_G$ and versus transport-voltage $V$ calculated along these lines is shown in Figure 11 as a grey-scale plot. Along the $V = 0$ axis the linear conductance peaks [7] can be seen with Coulomb blockade regions in between. The excitation spectrum of the quantum dot is reflected in the lines parallel to the Coulomb blockade areas at finite $V$ [37, 18]. Very similar figures have been obtained in experiments [16]. In Figure 11 the fine structure from Figure 7 has been taken as dot spectrum. The current is determined by the number of allowed transitions between excited dot states and jumps therefore step-like at low temperatures with changing gate- or transport-voltage. The conductance peaks e.g. split into a bar graph-like structure [10, 15]; its asymmetry is explained by unequal transmittivities $t_L \neq t_R$ [18, 38] and the reversal of the asymmetry with voltage is found experimentally [38]. Bright regions occur at finite $V$ and, in the example with unequal barriers shown in Figure 11, only on one voltage side. Only if the less transmittive barrier is attached to the lead with lower chemical potential electron escape transitions like ($i$) govern the current. On the other voltage side $N \longrightarrow N-1$ transitions still are fast compared to $N \longrightarrow N+1$ transitions.

Both interesting transport properties, the current depending on the direction of $V$ and the negative differential conductances, could be applied as mesoscopic rectifiers and mesoscopic oscillators, respectively.

The other type of transition that qualitatively influences transport by spin selection

rules is

(*ii*) $N$, ground state, $S \longrightarrow N \pm 1$, ground state, $S'$

if the total spins of the correlated electrons differ by more than $|S - S'| > 1/2$ [19]. (*ii*) concernes the only transition being relevant for linear transport. The dot is blocked in the $N$-electron ground state and the corresponding linear conductance peak is suppressed at zero temperature. Finite temperature or transport-voltage can involve excited states with appropriate spin values and the current becomes finite. The recovery of a conductance peak with temperature has been observed experimentally [39]. The second type (*ii*) of spin blockade can occur only in 2D quantum dots because the Lieb and Mattis-theorem guarantees ground state spin values 0 or $1/2$ in 1D (cf. Section 6.1). Thus in "slim" quantum dots no linear conductance peak should be "missing".

Ground state spin values differing by more than $1/2$ are shown in Figure 10. The transition between the $N = 4$ and $N = 5$ ground states is blocked in this example. Furthermore, the type (*ii*) spin blockades can cause negative differential conductances already at low transport-voltages close to the linear regime. These results are discussed in [19].

A magnetic field parallel to the 2D plane has only weak influence on the spatial part of the dot electron wave functions if the magnetic length remains large compared to the thickness of the 2D-electron gas. The main effect, a Zeeman-splitting of the quantum dot levels is observed [16, 37] by nonlinear transport spectroscopy. The calculation of the current according to (22) has been generalized [19] to consider all $(2S+1)$ Zeeman-levels separately. Two striking experimental observations can be explained within this model :

(a) The positions of the linear conductance peaks perform a zig-zag motion with magnetic field [39].

(b) The features of negative differential conductances vanish as the magnetic field exceeds a certain strength [40].

The Zeeman-splitting, linear with magnetic field, favours high spin states with their lowest $z$-components rather than low spin states. Therefore subsequent level crossings occur in the $N$- or the $N-1$-electron ground state so that the ground state spin values increase. The alternating values for the ground state spins explain the oscillation of the conductance peak position with magnetic field (a). Ultimately the spin polarized $S = N/2$ state becomes ground state. Due to spin blockade (*i*) this state shows low linear conductance. The excited states, which become involved at finite transport-voltages, are better conducting and the current rather increases than decreases. Negative differential conductances disappear and the second experimental observation (b) is explained.

## 8 Summary and Conclusions

The pocket state approximation presented in this article is particularly useful to describe the lowest, spin dependent excitations of a repulsively interacting few electron system in the highly correlated limit. This applies to single-electron experiments based on semiconductor heterostructures. The energy spectra differ qualitatively [41] from non-interacting situations. The lowest levels form multiplets and two types of excitations

reflect the importance of interactions. Both differ in their scaling from the $r_s^{-2}$ behaviour of excitation energies in absence of interactions. The spectrum is explained in terms of correlated many particle states. The distances between the multiplets correspond to vibrational excitations of localized electrons repelling each other by Coulomb forces. They can be viewed as the discrete excitation energies caused by the [ $N$- (in 1D) or $2N$-dimensional (in 2D)] confinement of *one* "pocket" of the interaction potential. These excitations are independent of the particle statistics (Fermions or Bosons). The internal splitting (fine structure) of each multiplet on the other hand is proportional to tunneling integrals between different pocket sites. Correlated motions connect different arrangements of the electrons and are therefore related to statistics and spin.

The fine structure and the spin values for a 1D square well potential are shown in Table 1 and Figure 7 up to $N \leq 6$. At sufficiently large $r_s$ only one tunneling integral $t_N$ exponentially dominates and determines the fine structure excitations. The ratios between them have been determined quantitatively. Their "universal" independence of the detailed form of the repulsion $w(x)$ between the electrons and of $r_s$ has been explained. By comparison with numerically obtained ratios the scale $r_c \approx 2\,a_B$ for the approach to the universal values agrees with [3, 25]. This scale characterizes the transition from the weakly interacting into the highly correlated system with its multiplet level structure. "Slim" quantum dots should behave effectively one-dimensional if they are narrower than the pocket state. The number of levels to a certain total spin $S$ within each multiplet can be given explicitly (18) for all electron numbers.

In presence of (discrete) symmetries of the 2D confining dot potential leading to $\nu > 1$ different classical electron ground states, the total number of eigenvalues in a multiplet is $\nu \cdot 2^N$. Such dependence of the fine structure spectra on the shape of the quantum dot can be relevant in experiments where a voltage is applied to side gates [42]. Experimentally the shape of the quantum dot is not rigidly fixed but depends on the distribution of surrounding (non-conducting) charges which itself may depend on the distribution of the (conducting) dot charges. In this way the dot electrons can adjust the environment to lower the total energy. For example, two electrons in a square will easily polarize their surrounding, leaving rather a diamond shaped configuration for the potential. The interplay between surrounding and granular electron density of the dot tends to reduce the number of equivalent minima in configuration space to the minimal value $N!$, the number of permutations of $N$ particles. Classical ground state energies being unequal only on the scale of the tunneling integral $t_N$ suffices. The symmetries which led to $\nu > 1$ thus are likely to be removed in polarizable environments.

In 2D the lowest eigenstates can be approximated within the pocket state basis if the inter-particle repulsion decays slower than $\sim |x|^{-2}$. Many of the qualitative results obtained in 1D are still valid in 2D. This concerns the scaling behaviour of the excitation energies and the "universality" of the rations between them. The highest state in the lowest vibrational multiplet is spin polarized if $\nu = 1$. As an example a square shaped quantum dot has been investigated. Ground state spin polarizations are found, being larger than the values $S = 0$ or $S = 1/2$ for non-interacting or 1D systems. The Lieb and Mattis-theorem is inapplicable to systems of higher dimensionality if $N > 2$. This property could perhaps be tested by sophisticated ESR-experiments [43] and should show up in the intensity of the linear conductance peaks.

Transitions between adjacent dot electron numbers in current carrying situations are restricted by spin selection rules. They qualitatively influence

1. the height of the linear conductance peaks
2. the nonlinear conductance properties.

Possible many electron excitations of the quantum dot lead to steps in the current when transport- or gate-voltages are changed. The differential conductances can even be negative [18]. The spin selection rules describe the experimentally observed non-linear transport properties [10, 11, 16] in a natural way which is otherwise difficult. A magnetic field oriented in the 2D plane leads to additional structure due to Zeeman splitting. With increasing strength of the field the conductance peaks oscillate in position and the features of negative differential conductances vanish within the spin blockade model [19]. Both behaviours agree with the magnetic field dependence found in recent experiments [39, 40].

## Acknowledgement

Many of the ideas and results presented here were obtained in collaboration with Dietmar Weinmann, Kristian Jauregui and Bernhard Kramer. The work profited a lot from fruitful discussions with Tobias Brandes, Walter Pfaff, Ulrich Weiss, Rolf Haug, Jürgen Weis (special thanks for the communication of experimental results prior to publication), Walter Apel and Alfred Hüller. Support has been received in part by the Deutsche Forschungsgemeinschaft via grant AP 47/1-1 and by the European Community within the SCIENCE program, grant SCC*-CT90-0020.

## Bibliography

[1] E. Wigner, Phys. Rev. **46**, 1002 (1934).

[2] D. M. Ceperley, B. J. Adler, Phys. Rev. Lett. **45**, 566 (1980).

[3] K. Jauregui, W. Häusler, B. Kramer, Europhys. Lett. **24**, 581 (1993).

[4] L. I. Glazman, I. M. Ruzin, B. I. Shklovskii, Phys. Rev. **B 45**, 8454 (1992).

[5] D. V. Averin, Yu. V. Nazarov, Phys. Rev. **B 47**, 9944 (1993).

[6] D. V. Averin, K. K. Likharev in : *Quantum Effects in Small Disordered Systems*, ed. by B. L. Altshuler, P. A. Lee, R. A. Webb (Elsevier, Amsterdam, 1991);
G. Schön, A. D. Zaikin, Phys. Rep. **198**, 237 (1990);
H. Grabert, G. L. Ingold, M. H. Devoret, D. Esteve, H. Pothier, C. Urbina, Z. Phys. **B 84**, 143 (1991);
A good review can be found in : H. Grabert, M. Devoret, editors, *Single Charge Tunneling* NATO ASI Series, Plenum Press, volume 294 (1992).

[7] U. Meirav, M. A. Kastner, S. J. Wind, Phys. Rev. Lett. **65**, 771 (1990).

[8] Special Issue on *Single Charge Tunneling* edited by H. Grabert, Z. Phys. **B 85**, 317-468 (1991).

[9] M. A. Kastner, Rev. Mod. Phys. **64**, 849 (1992).

[10] A. T. Johnson, L. P. Kouwenhoven, W. de Jong, N. C. van der Vaart, C. J. P. M. Harmanns, C. T. Foxon, Phys. Rev. Lett. **69**, 1592 (1992).

[11] J. Weis, R. J. Haug, K. v. Klitzing, K. Ploog, Phys. Rev. **B 46**, 12837 (1992).

[12] Proceedings of the Conference *The Physics of Few-Electron Nanostructures*, Noordwijk, Physica **B 189**, 1-277 (1993).

[13] Ch. Sikorski, U. Merkt, Phys. Rev. Lett. **62**, 2164 (1989);
B. Meurer, D. Heitmann, K. Ploog, Phys. Rev. Lett. **68**, 1371 (1992);
R. C. Ashoori, H. L. Stormer, J. S. Weiner, L. N. Pfeiffer, S. J. Pearton, K. W. Baldwin, K. W. West, Phys. Rev. Lett. **68**, 3088 (1992);
R. C. Ashoori, H. L. Stormer, J. S. Weiner, L. N. Pfeiffer, K. W. Baldwin, K. W. West, Phys. Rev. Lett. **71**, 613 (1993).

[14] D. Pfannkuche, R. R. Gerhards, Phys. Rev. **B 44**, 13132 (1991).

[15] D. V. Averin, A. N. Korotkov, Journ. of Low Temp. Phys. **80**, 173 (1990);
D. V. Averin, A. N. Korotkov, K. K. Likharev, Phys. Rev. **B 44**, 6199 (1991);
E. B. Foxman, P. L. McEuen, U. Meirav, N. S. Wingreen, Y. Meir, P. A. Belk, N. R. Belk, M. A. Kastner, S. J. Wind, Phys. Rev. **B 47**, 10020 (1993).

[16] J. Weis, R. J. Haug, K. v. Klitzing, K. Ploog, Phys. Rev. Lett. **71**, 4019 (1993).

[17] W. Häusler, K. Jauregui, D. Weinmann, T. Brandes, B. Kramer, Physica **B 194-196**, 1325 (1994)

[18] D. Weinmann, W. Häusler, W. Pfaff, B. Kramer, U. Weiss, to appear in Europhys. Letters (1994).

[19] D. Weinmann, W. Häusler, B. Kramer, unpublished.

[20] C. W. J. Beenakker, Phys. Rev. **B 44**, 1646 (1991).

[21] U. Merkt, J. Huser, M. Wagner, Phys. Rev. **B 43**, 7320 (1991).

[22] P. Hawrylak, D. Pfannkuche, Phys. Rev. Lett. **70**, 485 (1993).

[23] G. W. Bryant, Phys. Rev. Lett. **59**, 1140 (1987).

[24] W. Häusler, B. Kramer, J. Mašek, Z. Phys. **B 85**, 435 (1991).

[25] W. Häusler, B. Kramer, Phys. Rev. **B 47**, 16353 (1993).

[26] P. Maksym, Physica **B 184**, 385 (1993).

[27] G. Meissner, H. Namaizawa, M. Voss, Phys. Rev. **B 13**, 1370 (1976).

[28] D. Pfannkuche, V. Gudmundsson, P. A. Maksym, Phys. Rev. **B 47**, 2244 (1993).

[29] J. Mašek, unpublished.

[30] E. Lieb, D. Mattis, Phys. Rev. **125**, 164 (1962).

[31] A. Hüller, D. M. Kroll, J. Chem. Phys. **63**, 4495 (1975).

[32] M. Hamermesh : *"Group Theory and its Applications to Physical Problems"*, new edition, Dover Publications, New York (1989).

[33] Bjørn Felsager : *"Geometry, Prticles and Fields"*, Odense University Press (1981).

[34] T. Inui, Y. Tanabe, Y. Onodera : *"Solid State Sciences"*, Springer, Berlin (1990).

[35] K. Moulopoulos, N. W. Ashcroft, Phys. Rev. Lett. **69**, 2555 (1992).

[36] C. Bruder, H. Schoeller, Phys. Rev. Lett. **72**, 1076 (1994).

[37] J. Weis, PhD thesis, University of Stuttgart (1994).

[38] N. C. van der Vaart, A. T. Johnson, L. P. Kouwenhoven, D. J. Maas, W. de Jong, M. P. de Ruyter van Steveninck, A. van der Enden, C. J. P. M. Harmanns, in Ref. [12], p. 99.

[39] J. T. Nicholls, J. E. F. Frost, M. Pepper, D. A. Ritchie, M. P. Grimshaw, G. A. Jones, Phys. Rev. **B 48**, 8866 (1993).

[40] J. Weis, R. J. Haug, private communication.

[41] J. J. Palacios, L. Martin-Moreno, C. Tejedor, Europhys. Lett. **23**, 495 (1993).

[42] L. P. Kouwenhoven, PhD thesis, Technical University of Delft (1992).

[43] R. N. Ghosh, R. H. Silsbee, Phys. Rev. **B 46**, 12508 (1992).